NASA/TM—2000-210347

Recommendations for Achieving Accurate Numerical Simulation of Tip Clearance Flows in Transonic Compressor Rotors

Dale E. Van Zante, Anthony J. Strazisar, and Jerry R. Wood
Glenn Research Center, Cleveland, Ohio

Michael D. Hathaway
U.S. Army Research Laboratory, Glenn Research Center, Cleveland, Ohio

Theodore H. Okiishi
Iowa State University, Ames, Iowa

September 2000

The NASA STI Program Office . . . in Profile

Since its founding, NASA has been dedicated to the advancement of aeronautics and space science. The NASA Scientific and Technical Information (STI) Program Office plays a key part in helping NASA maintain this important role.

The NASA STI Program Office is operated by Langley Research Center, the Lead Center for NASA's scientific and technical information. The NASA STI Program Office provides access to the NASA STI Database, the largest collection of aeronautical and space science STI in the world. The Program Office is also NASA's institutional mechanism for disseminating the results of its research and development activities. These results are published by NASA in the NASA STI Report Series, which includes the following report types:

- TECHNICAL PUBLICATION. Reports of completed research or a major significant phase of research that present the results of NASA programs and include extensive data or theoretical analysis. Includes compilations of significant scientific and technical data and information deemed to be of continuing reference value. NASA's counterpart of peer-reviewed formal professional papers but has less stringent limitations on manuscript length and extent of graphic presentations.

- TECHNICAL MEMORANDUM. Scientific and technical findings that are preliminary or of specialized interest, e.g., quick release reports, working papers, and bibliographies that contain minimal annotation. Does not contain extensive analysis.

- CONTRACTOR REPORT. Scientific and technical findings by NASA-sponsored contractors and grantees.

- CONFERENCE PUBLICATION. Collected papers from scientific and technical conferences, symposia, seminars, or other meetings sponsored or cosponsored by NASA.

- SPECIAL PUBLICATION. Scientific, technical, or historical information from NASA programs, projects, and missions, often concerned with subjects having substantial public interest.

- TECHNICAL TRANSLATION. English-language translations of foreign scientific and technical material pertinent to NASA's mission.

Specialized services that complement the STI Program Office's diverse offerings include creating custom thesauri, building customized data bases, organizing and publishing research results . . . even providing videos.

For more information about the NASA STI Program Office, see the following:

- Access the NASA STI Program Home Page at ***http://www.sti.nasa.gov***

- E-mail your question via the Internet to help@sti.nasa.gov

- Fax your question to the NASA Access Help Desk at (301) 621-0134

- Telephone the NASA Access Help Desk at (301) 621-0390

- Write to:
  NASA Access Help Desk
  NASA Center for AeroSpace Information
  7121 Standard Drive
  Hanover, MD 21076

NASA/TM—2000-210347

Recommendations for Achieving Accurate Numerical Simulation of Tip Clearance Flows in Transonic Compressor Rotors

Dale E. Van Zante, Anthony J. Strazisar, and Jerry R. Wood
Glenn Research Center, Cleveland, Ohio

Michael D. Hathaway
U.S. Army Research Laboratory, Glenn Research Center, Cleveland, Ohio

Theodore H. Okiishi
Iowa State University, Ames, Iowa

Prepared for the
International Gas Turbine Institute Exposition
sponsored by the American Society of Mechanical Engineers
Indianapolis, Indiana, July 7–10, 1999

National Aeronautics and
Space Administration

Glenn Research Center

September 2000

Acknowledgments

The authors wish to thank Tim Beach for his assistance with grid generation, John Adamczyk for much assistance in interpreting the solutions, Aamir Shabbir for assistance with the LSAC and design speed Rotor 35 solutions, Mark Celestina for guidance in running APNASA, and Nick Cumpsty for useful discussions. The first author thanks the National Research Council for their sponsorship.

Available from

NASA Center for Aerospace Information
7121 Standard Drive
Hanover, MD 21076
Price Code: A03

National Technical Information Service
5285 Port Royal Road
Springfield, VA 22100
Price Code: A03

Available electronically at http://gltrs.grc.nasa.gov/GLTRS

Recommendations for Achieving Accurate Numerical Simulation of Tip Clearance Flows in Transonic Compressor Rotors

Dale E. Van Zante, Anthony J. Strazisar and Jerry R. Wood
National Aeronautics and Space Administration
Glenn Research Center
Cleveland, OH

Michael D. Hathaway
U.S. Army Research Laboratory
National Aeronautics and Space Administration
Glenn Research Center
Cleveland, OH

Theodore H. Okiishi
Iowa State University
Ames, IA

ABSTRACT

The tip clearance flows of transonic compressor rotors are important because they have a significant impact on rotor and stage performance. While numerical simulations of these flows are quite sophisticated, they are seldom verified through rigorous comparisons of numerical and measured data because these kinds of measurements are rare in the detail necessary to be useful in high-speed machines. In this paper we compare measured tip-clearance flow details (e.g. trajectory and radial extent) with corresponding data obtained from a numerical simulation. Recommendations for achieving accurate numerical simulation of tip clearance flows are presented based on this comparison. Laser Doppler Velocimeter (LDV) measurements acquired in a transonic compressor rotor, NASA Rotor 35, are used. The tip clearance flow field of this transonic rotor was simulated using a Navier-Stokes turbomachinery solver that incorporates an advanced k-ε turbulence model derived for flows that are not in local equilibrium. Comparison between measured and simulated results indicates that simulation accuracy is primarily dependent upon the ability of the numerical code to resolve important details of a wall-bounded shear layer formed by the relative motion between the over-tip leakage flow and the shroud wall. A simple method is presented for determining the strength of this shear layer.

INTRODUCTION

Tip clearance flows are of great engineering importance when designing modern axial fans and compressors because of their large impact on pressure rise, efficiency, and stability Wisler (1985), Adamczyk et al. (1993), Hoying et al. (1998).

In recent years Navier-Stokes (NS) codes have become a common component of most modern design systems and attention has turned toward obtaining accurate clearance flow simulations using these codes. Detailed measurements obtained in 1994 on NASA Rotor 37 provided the turbomachine flow simulation community with the data necessary for CFD code assessment in the blade tip region of transonic compressors. These measurements have been used in code assessment efforts organized by ASME (Denton, 1996) and AGARD (Dunham and Meauze, 1998; AGARD, 1998). Suder and Celestina (1996), Chima (1998), Gerolymos and Vallet (1998), and others have also used these measurements specifically to assess the accuracy of rotor tip clearance flow predictions.

These code assessment exercises show that CFD simulations generally overpredict the temperature rise in the outer 10% of span when compared to measurements acquired far downstream of the rotor. This leads to an underprediction of overall efficiency. A general recommendation coming from these exercises is that turbulent transport models result in more accurate clearance flow simulations than algebraic mixing length turbulence models because of the multiple length scales which exist in the clearance flow region. However, no clear recommendations about the grid topology or grid resolution required for accurate simulation of the tip clearance flow have yet emerged.

Whether or not accurate clearance flow simulations require gridding of the tip clearance gap at all, and if so how much gridding, is still an open issue. Currently there are three general methods for treating the tip clearance gap: i) assuming flow periodicity across a non-gridded region above the blade tip (Kirtley et al., 1990); ii) rounding the blade tip by distorting an H-type grid to fill the gap over the blade (Dawes, 1987); iii) fully gridding the gap with a separate grid block. The ability to obtain accurate simulations with minimal or no gridding is desirable because gridding the gap requires increased computational resources due to the added complexity of multiple grid blocks and also increases the total number of grid points (30,000 additional grid points by Chima and 270,000 by Gerolymos and Vallet).

The objectives of the present effort are as follows:

- Determine the grid topology and density which results in an accurate simulation of the tip clearance flow
- Assess the accuracy of the predicted temperature rise near the blade tip using measurements acquired within the blade row instead of measurements acquired far downstream of the blade

These objectives are met using a 3D Navier-Stokes solver that incorporates an advanced k-ε turbulence model derived for flows that are not in local equilibrium. Predictions are compared to laser anemometer data acquired at several axial locations within the blade passage of a transonic compressor. The laser data used in the present investigation provide a more complete view of clearance flow development than possible with the NASA Rotor 37 data used by previous investigators. The Euler turbine equation is used to calculate the temperature rise within the clearance flow from measured tangential velocity data, providing a more accurate assessment of the CFD-predicted temperature rise than obtained from aerodynamic probe measurements acquired far downstream of the rotor.

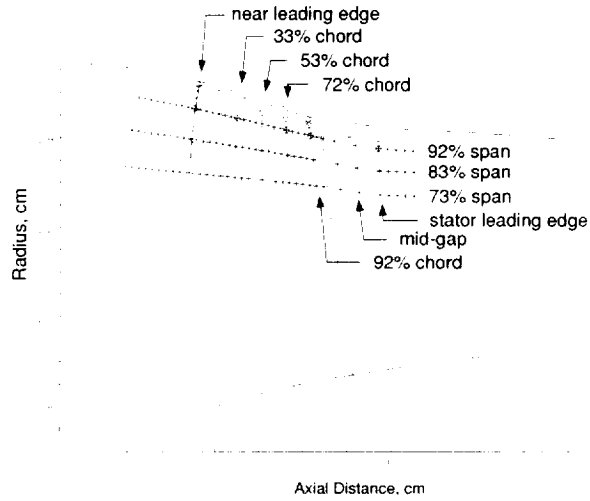

FIGURE 1. LDV measurement locations for Rotor 35.

EXPERIMENT

LDV measurements were acquired in the NASA Lewis single-stage axial-flow compressor facility using NASA Rotor 35 operating in a rotor-only (no stator) configuration. The rotor has 36 blades, a hub-tip radius ratio of 0.70, an aspect ratio of 1.19, a tip solidity of 1.3, and an axial chord of 4.12 cm at the hub. The design and blade coordinates are found in Reid and Moore (1978). Data was acquired at a tip speed of 363 m/s (80% design speed) at the near peak efficiency operating condition. The total pressure ratio and efficiency at this operating condition are 1.44 and 92% respectively. This operating condition was dictated by requirements for rotor/stator matching in a follow-on stage investigation as reported by Van Zante, et al. (1997).

The nominal tip clearance as measured with touch probes was 0.74 mm, which corresponds to 1.3% of rotor tip chord and 1% of rotor leading edge span. The touch probes only measure the "tallest" blade and provide no information about how similar the tallest blade is to the majority of blades or about the magnitude of variations in blade height. Blade heights for Rotor 37 were measured at the completion of testing as part of the ASME test case geometry documentation. Since Rotor 37 and Rotor 35 were designed and manufactured at the same time, the results of Rotor 37 blade height measurements are considered representative for Rotor 35. In the present investigation, blade height uniformity is most important at the rotor leading edge since this is the region that most influences the clearance flow. For Rotor 37, 21 of the 36 blade heights were within 0.051mm (7% nominal gap height) of each other at the leading edge, which indicates good blade-to-blade uniformity. The difference in height between the tallest blade and the average of the group of 21 was 0.076mm (10% nominal gap height) which indicates that the nominal clearance value is representative of the majority of blades for Rotor 37. Rotor 35 can be expected to exhibit similar results. In addition, detailed analysis of LDV measurements from individual blade passages (which is not presented herein) indicates no strong passage-to-passage flow field variations near the blade tip. The results presented herein, which are based on measurements and predictions for an "average" blade passage, are therefore considered to be representative of individual blade passages as well.

The compressor rotor massflow was measured using a calibrated orifice plate located far upstream of the compressor. Performance measurements were acquired using conventional static pressure and total pressure/temperature probes located upstream and downstream of the rotor. Overall performance was calculated by mass-averaging total temperature and energy-averaging total pressure across the annulus (Strazisar, et al., 1989; Reid and Moore, 1978). Measurement uncertainties are: massflow +/- 0.3kg/s, flow angle +/- 0.5 degrees, total pressure +/- 100Pa, total temperature +/- 0.6K.

A large window, which conformed to the 3D shroud contour, provided optical access to the flowfield from one rotor chord upstream of the rotor to two rotor chords downstream. LDV measurements were made in detail in the outer 20% of span; see Fig. 1. Streamsurface surveys (+ symbols) were acquired at 73, 83, and 92% span. Crosschannel surveys (diamond symbols) were acquired near the leading edge, 33, 53, 72, and 92% rotor chord. Although the stator was not installed, measurements were also acquired at the axial locations corresponding to mid rotor/stator gap and to the stator leading edge to assess what the tip flow field would be at these locations in the stage environment. The uncertainty in the LDV measurements is approximately +/- 1.0 m/s for absolute velocity and +/- 0.5 degrees in absolute flow angle.

The LDV was configured as a two-channel laser system that acquired axial and tangential velocities simultaneously. For each velocity measurement the rotor position was determined from a shaft angle encoder and the data placed into the window corresponding to that shaft angle position. There were 184 windows across one rotor blade pitch. Typically 40,000 to 60,000 individual velocity measurements were acquired for each survey point. Since the measurements were not evenly distributed over all of the windows, the total number of measurements was chosen so as to insure that there was a minimum of 30 measurements in any win-

dow. The LDV data were ensemble averaged using one rotor blade pitch as the length scale. See Strazisar et al. (1989) for more detail on the LDV data acquisition and reduction technique.

LDV data

Figure 2 shows contours of axial velocity for the 92% span streamsurface which illustrate the lower extent of the flowfield region impacted by the tip clearance flow. Axial velocity is chosen here since the footprint of the clearance flow shows most clearly as gradients in axial velocity on this streamsurface. The projection of the clearance flow trajectory as determined from a detailed analysis of the measurements acquired across the blade pitch at different axial locations is superimposed on the contours as a dashed line. A passage shock can clearly be seen in the figure. Although the rotor is operating near peak efficiency, the shock is spilled forward of the leading edge because the rotor is operating at a part-speed condition.

Crosschannel contour plots of the absolute tangential velocity over the outer 20% of the blade span, Fig. 3, provide a more quantitative view of the trajectory and radial extent of the clearance flow. The clearance flow appears as a region of high absolute tangential velocity. The high tangential velocity fluid in the clearance flow also has a high total temperature (which can be shown by using the Euler turbine equation). As we will show later, the trajectory of this high total temperature fluid plays an important role in determining the total temperature rise near the blade tip. The tip clearance flow extends radially to 92% span at the 33% chord plane. This radial extent remains relatively constant as the clearance flow convects downstream.

The clearance flow pattern immediately downstream of the clearance flow/shock interaction that occurs near mid pitch is shown on the crosschannel plane at 33% rotor chord. Further downstream the clearance flow migrates toward the pressure surface of the adjacent blade, but does not accumulate on the pressure surface, as shown by the 92% chord plane data. The tip clearance flow then merges with the rotor wake downstream of the rotor as shown by the data acquired at the mid rotor/stator gap location in Fig. 3 (note the color scale change).

Also visible at 92% chord is a second region of elevated tangential velocity adjacent to the suction surface of the blade at the tip. This region is formed when clearance flow fluid from the adjacent passage leaks across the blade tip. We will refer to this feature as the secondary clearance flow to distinguish it from the primary clearance flow that accumulates in the pressure-surface/shroud corner of the passage. The secondary clearance flow is also visible at the mid rotor/stator gap axial location and has migrated toward the pressure side of the adjacent blade passage. The secondary clearance flow was first identified by Suder and Celestina (1996) in measurements and simulations of part-speed operating conditions in NASA Rotor 37. They attributed its presence to the entrainment of radially-migrating suction surface boundary layer fluid by the over-tip leakage flow in the rear of the blade passage. This secondary clearance flow is also present in the Rotor 37 design-speed simulation of Gerolymos and Vallet (1998), who also predicted suction surface boundary layer migration near the tip of the blade. However, blade boundary layer migration is not

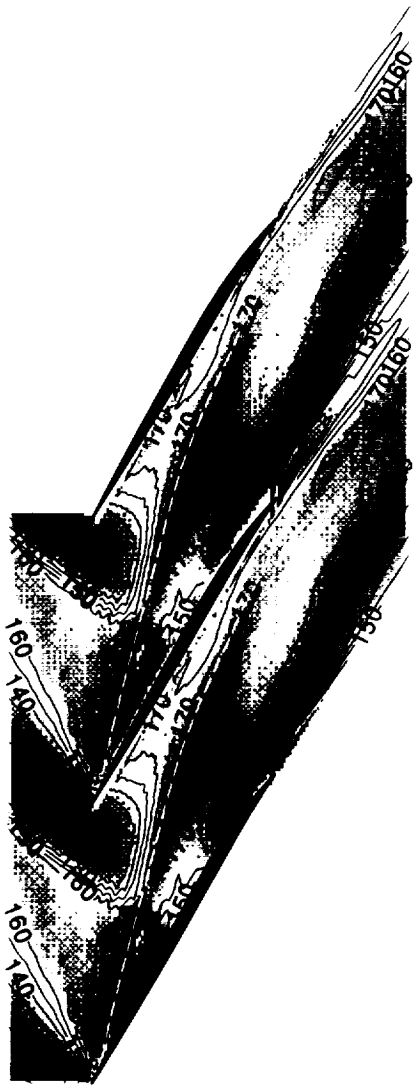

FIGURE 2. Contours of axial velocity (m/s) on the 92% span streamsurface from the LDV measurements. The clearance flow trajectory is marked by the dashed line.

predicted by any of our simulations. The secondary clearance flow therefore appears to be generic, is due to over-tip leakage flow in the rear portion of the blade passage, and is not dependent on migration of suction surface boundary layer fluid.

NAVIER STOKES SIMULATIONS

Three-dimensional time-averaged Navier-Stokes simulations of the flow through the compressor rotor operating at near peak efficiency were generated using the Average Passage code (APNASA Version 1.11) developed by Adamczyk (1990). The turbulence model used in the simulations was developed by the Center for Modeling of Turbulence and Transition at NASA Lewis

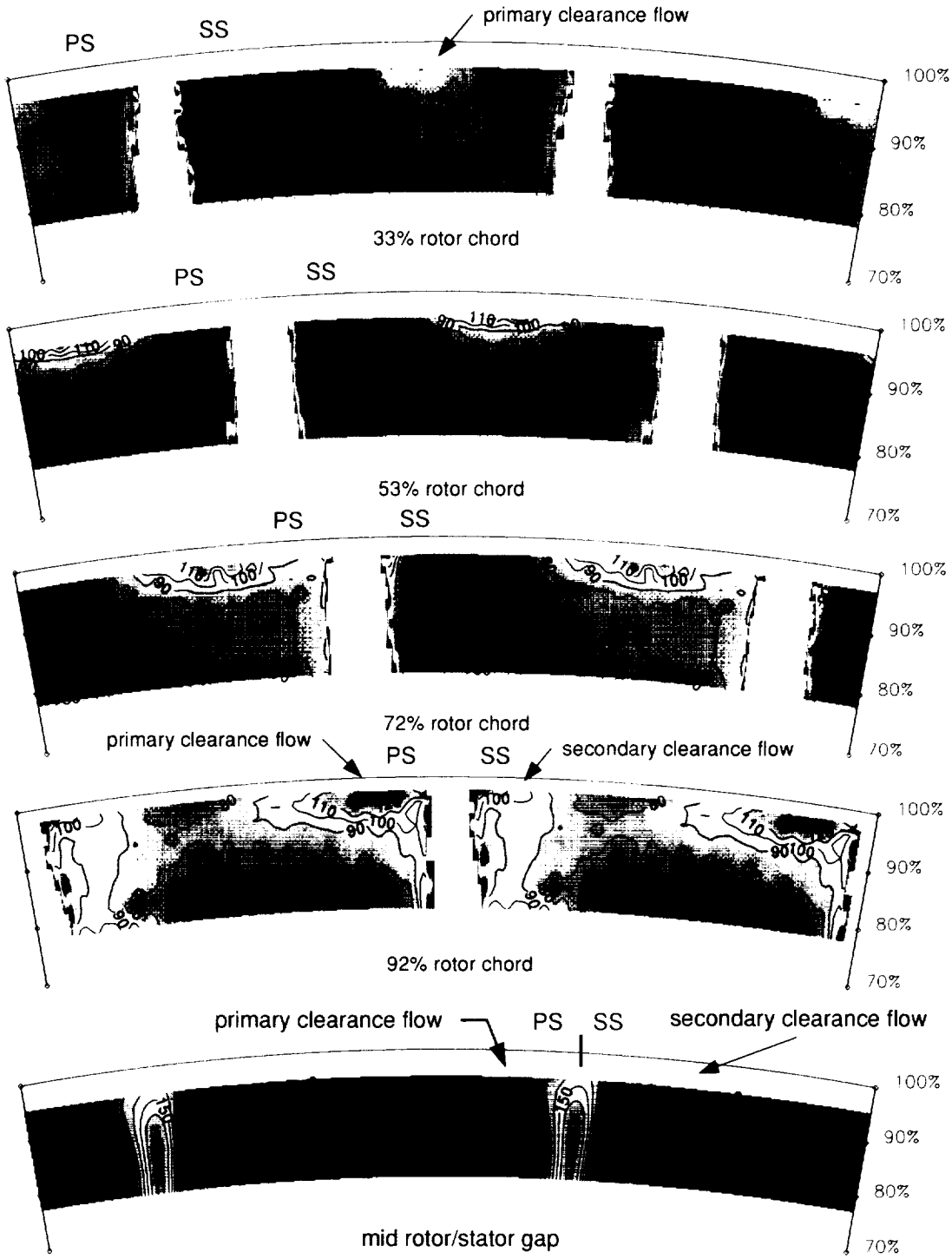

FIGURE 3. Contours of tangential velocity (m/s) at 33, 53, 72, 92% rotor chord and mid-gap from the LDV measurements.

and is a refinement of the standard k-ε model. This refined model overcomes some of the deficiencies of the standard k-ε model for flows that are not in local equilibrium. Details of the model and its implementation in the Average Passage code are discussed in Shabbir et al. (1996).

A NASTRAN analysis of the rotor was performed for the

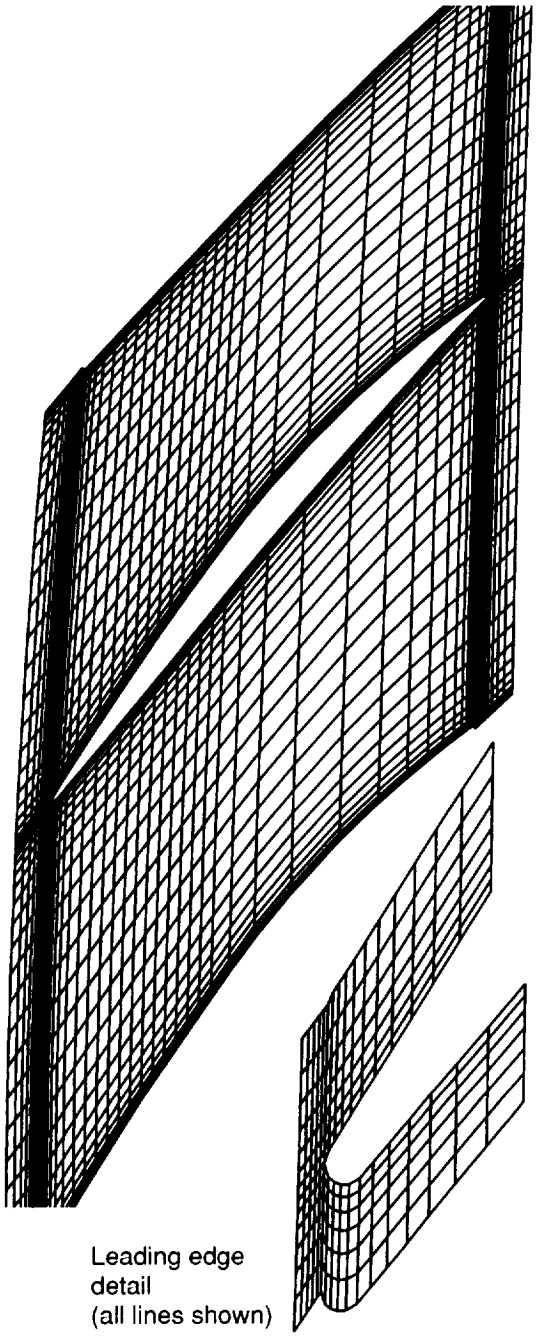

FIGURE 4. Detail of rotor mesh at 50% span (every other grid line is shown).

80% speed peak efficiency operating condition at which the LDV data were acquired so that the cold blade coordinates could be corrected for pressure, temperature, and centrifugal load deflections. This corrected "as running" geometry was used for the Navier-Stokes simulations.

Shabbir et al. (1997) showed that leakage flow from an axial

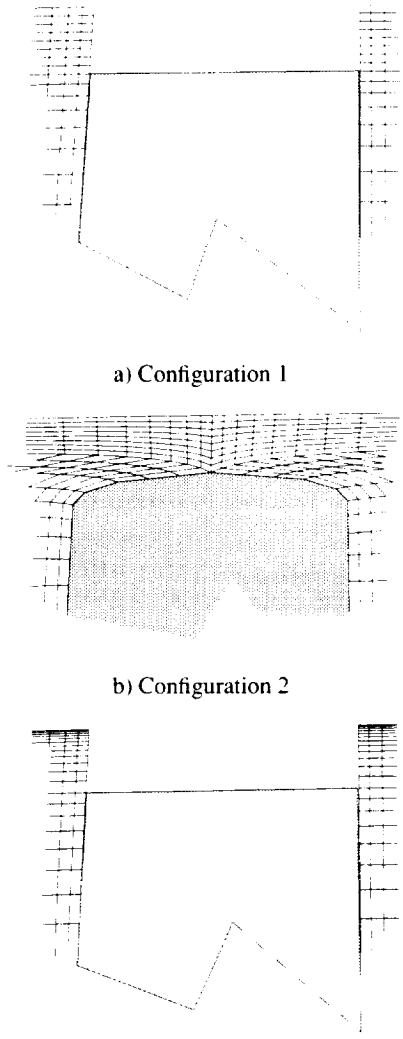

a) Configuration 1

b) Configuration 2

c) Configuration 3

FIGURE 5. Detail of mesh in the blade tip region.

gap between the rotor disk and the non-rotating hub flowpath upstream of the rotor can impact the axisymmetric flow over the entire span of this rotor. This effect arises from pumping of the blind cavity beneath this gap and is present even for zero net leakage flow through the gap. This effect was therefore modeled in the present work using Shabbir's scheme with the assumption of a net leakage of 0.25% of the throughflow, which Shabbir found to give the best agreement between simulated and measured performance at 80% speed.

While several grid methodologies are explored in this work, the overall character of the grids is similar for each method with variations between grids confined to the tip clearance region. A sheared H-grid topology is used. The blade to blade grid, shown in Fig. 4, is aligned with the blade camber angle near the leading edge and slowly turns to axial far upstream of the blade. This grid approximately follows the blade camber angle downstream of the

Table 1: Summary of clearance gap and grid topology variations investigated.

Configuration	Clearance full= 1.3% of chord	Number of cells in gap	Gap gridded or modeled	Radial grid spacing in the clearance gap
1	Uniform, full	8	modeled	Constant cell size
2	Uniform, full	8	gridded	Same as Configuration 1
3	Uniform, full	12	modeled	Clustered at the shroud
4	Uniform, full	12	gridded	Same as Configuration 3
5	Uniform, 1/2	8	modeled	Same as Configuration 3
6	Non-uniform: 1/2 to full	8	modeled	Same as Configuration 3
7	Non-uniform: 3/4 to full	8	modeled	Same as Configuration 3

blade. The grid has 71 nodes along the blade chord which includes 10 nodes each on leading and trailing edge circles, 67-75 nodes radially from the hub to the blade tip, and 51 nodes pitchwise. The axial grid density is doubled in the first 50% of rotor chord (to an average node spacing of 1.32% chord) to better define the passage shock.

Tip grid topology

Simulations were generated using several different grids in the clearance gap region for several clearance height variations to determine the most accurate simulation methodology. The grid and clearance variations are summarized in Table 1 and Fig. 5. These variations of gridding were designed to help resolve the following issues:

- the effect of modeling versus gridding the tip clearance gap
- the effect of the near-shroud grid cell size in the radial direction
- the effect of changing the tip clearance height with uniform height along the blade chord
- the effect of changing the tip clearance height non-uniformly along the chord

The baseline tip gridding scheme used in the present work is that proposed by Kirtley et al. (1990). A view of this type of tip grid, used in Configurations 1,3,5,6,7 (see Table 1), is shown in Fig. 5a. This efficient scheme uses a periodic boundary across a non-gridded region over the top of the blade tip to treat the clearance flow as an orifice flow with no change in mass, momentum, or energy across the blade tip. The region from the blade tip to the shroud is constructed by extending the grid from below the blade tip to the shroud while maintaining the tangential thickness of the blade. A benefit of this method is that it is simple to implement, since it does not require a multi-block grid topology or solver. Drawbacks include that the blade tip is implicitly assumed to be square edged, the over-tip leakage flow direction is assumed normal to the blade pressure surface (no chordwise movement of clearance flow is allowed), and a discharge coefficient must be chosen to account for any vena contracta in the over-tip leakage flow.

Tip grid Configuration 2, shown in Fig. 5b, was generated to investigate differences between a fully-gridded tip gap and the modeled gap treatment. This grid employs the same radial spacing in the clearance gap as that used for Configuration 1. The blade corners are rounded in this grid to avoid using a multi-block topology. The blade corner radius used was approximately 0.1 mm. This radius was measured on NASA Rotor 37 (AGARD, 1998), which has the same aspect ratio, blade chord, tip speed, and flowpath as Rotor 35. Since Rotors 35 and 37 are so similar in design, they can be expected to exhibit the same blade tip erosion characteristics. The Rotor 37 blade corner radius is therefore considered to be a good approximation to the Rotor 35 corner radius.

To investigate the effect of the near-shroud grid density, a third grid (Configuration 3) was generated with 12 grid cells non-uniformly spaced in the tip gap. This grid is shown in Fig. 5c. Grid cells in the tip gap are clustered at the shroud and stretched toward the blade tip to maintain nearly the same number of cells on the blade span without violating standard grid stretching rules. This results in a cell size in the radial direction at the shroud which is only one-fourth of that used in Configuration 1 and a smooth stretching ratio variation from the tip gap to the blade. The pitchwise and chordwise grid spacings remained identical to those used previously.

Chima (1998) compared a fully-gridded simulation of the tip gap to a modeled simulation for Rotor 37 at design speed. The fully-gridded simulation indicated an expansion of the over-tip leakage flow around the pressure surface/blade tip corner which caused the leakage flow to entirely fill the clearance gap. Gerolymos and Vallet (1998) found a similar result. Based on these studies, we assume that a vena contracta does not exist in the over-tip leakage flow. A discharge coefficient of 1.0 is therefore used for all simulations in which the gap is modeled.

RESULTS

Near-wall grid spacing effects

Simulations generated with tip grid Configurations 1 and 3

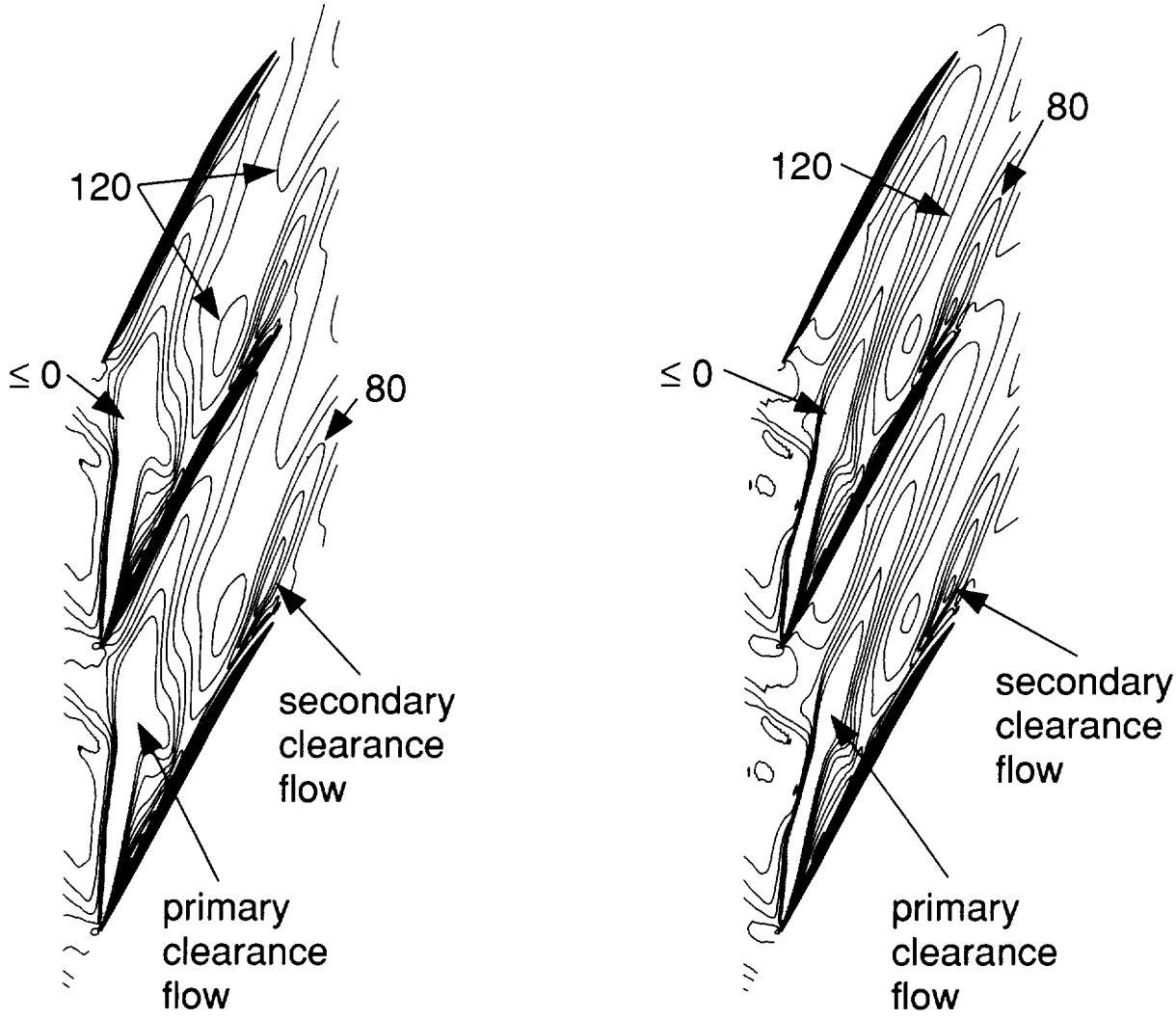

a) Configuration 1

b) Configuration 3

FIGURE 6. Axial velocity contours (starting at 0 m/s with 20 m/s intervals) for the blade tip grid plane for configurations 1 and 3.

were compared to assess the impact of the near-shroud grid spacing on simulation fidelity. Solutions for these two cases were converged to the same operating condition near peak efficiency. The predicted tip clearance flow trajectory and penetration are shown in Figs. 6 and 7 respectively. The trajectory of the clearance flow is illustrated in Fig. 6 using contour plots of the axial velocity on the grid plane corresponding to the blade tip. The clearance flow is indicated by two areas of low axial velocity: the shaded region denotes where the axial velocity is less than zero in the primary clearance flow, while the secondary clearance flow is identified as a locus of low axial velocity near the blade trailing edge. Comparison between Figs. 6a and 6b indicates that the clearance flow trajectory is more inclined in the streamwise direction when the near-shroud grid spacing is reduced. The clearance flow no longer impacts the pressure surface of the blade near mid-chord, but rather turns to be more parallel to the pressure surface, which is in closer agreement with the measured result shown in Fig. 2. The reason for this change in trajectory is described in the *Discussion* section below.

The radial penetration of the clearance flow is shown in Fig. 7. Fluid from the primary clearance flow appears as a region of high tangential velocity (and also high total temperature) near the corner formed by the shroud and the pressure surface in the rear of the rotor blade passage. Fluid from the secondary clearance flow can also be seen in the suction surface shroud corner. For Configuration 1 (Fig. 7a) the primary clearance flow fluid appears closer to the blade pressure surface and has penetrated to lower immersions than shown by the measurements in Fig. 3. Predicted results

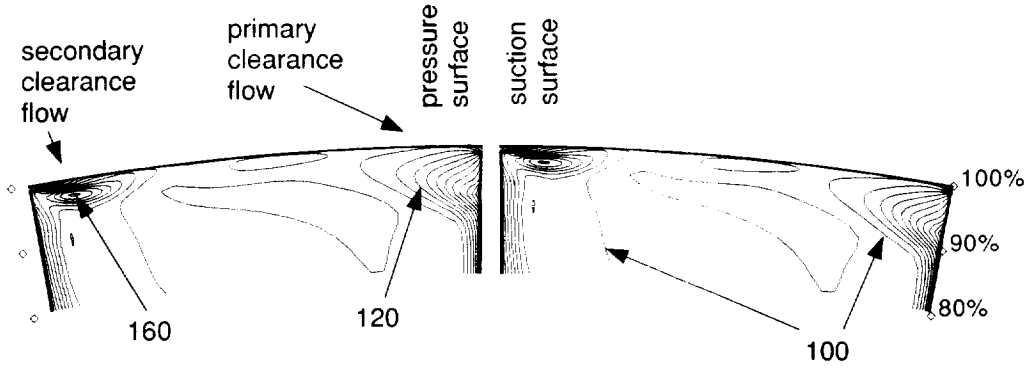

a) Configuration 1

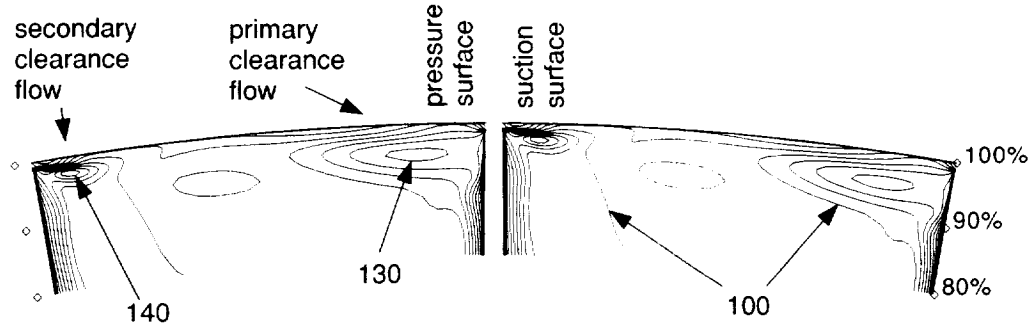

b) Configuration 3

FIGURE 7. Tangential velocity contours (10 m/s interval) for the outer 20% of span on the crosschannel surface at 92% rotor chord for configurations 1 and 3.

downstream of the rotor (which are not shown here) also indicate that the clearance flow merges with the pressure side of the blade wake for Configuration 1 and mixes quite slowly downstream of the rotor. This behavior does not agree with that observed in the measurements since the data shown in Fig. 3 at the mid rotor/stator gap location show little indication of a well-defined clearance flow region.

Comparison between the results in Figs. 7a and 7b indicates that a reduction in the near-shroud grid spacing brings the simulation closer to the data. However, the simulated primary clearance flow still displays a tendency to accumulate on the pressure surface in the rear of the blade passage that is not reflected in the measurements.

Modeled versus gridded clearance gap

The solutions generated with tip grid Configurations 2 and 4 were used to assess the accuracy of the modeling methodology proposed by Kirtley et al. (1990) and also the impact of rounded blade corners on the amount of over-tip leakage flow. The trajectory and radial penetration of the clearance flow for Configurations 1 and 2 were not significantly different. The same was true when results from Configurations 3 and 4 were compared. Gridded gap results are therefore not shown herein. Calculation of the mass flow through the clearance gap indicates that the gridded gap cases allowed 30% more flow through the gap than the modeled cases. In summary, rounding the blade tip and gridding the tip gap are not major influences on solution fidelity.

Clearance height effects

The tip contour of Rotor 35 and the contour of the outside of the window were measured with the LDV system. Although it is not possible to determine the actual value of clearance height from these measurements, it is possible to infer the relative variation of clearance height with rotor chord. These measurements indicate that the clearance height at the rotor leading edge is 20-25% less than at the blade trailing edge as shown in Fig. 8. The nominal clearance height was 0.74 mm. The error bars denote the uncertainty in clearance height as determined with the LDV system. This uncertainty is relatively large because the LDV system has poor spatial resolution in the radial direction when focussed near the window due to strong reflections from the window and blade tip surfaces. Despite the inability to measure the exact variation of clearance with chord in the experiment, it is clear that a non-uniform clearance along the chord exists in the experiment.

To determine the influence of clearance height variation on simulation accuracy, three additional simulations were performed. The 12-cell simulation (Configuration 3) performed for the full clearance height indicates a slightly higher accumulation of clear-

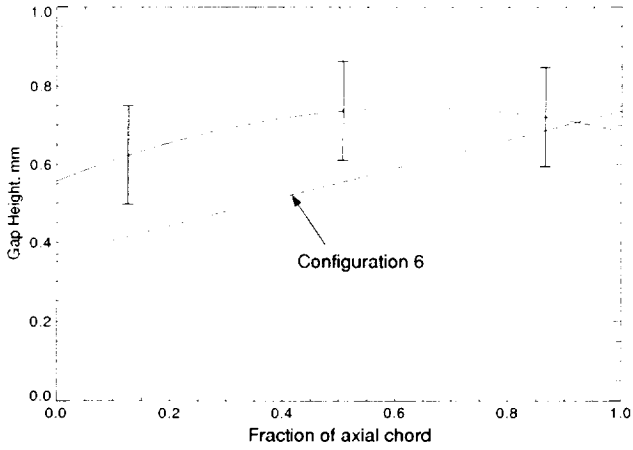

FIGURE 8. Tip gap height versus rotor axial chord as inferred from the LDV system measurements is shown as a solid line. The tip clearance gap height used for configuration 6 is shown as a dashed line.

ance flow fluid in the pressure surface shroud corner than was measured (compare Figs. 7b and 3). A reduction in the tip clearance height will result in a reduction in the amount of over-tip leakage flow. Configuration 5, in which the clearance gap was reduced uniformly along the chord by 50%, was performed to assess the impact of this change on the strength of the clearance flow. Non-uniform clearance height effects similar to those present in the experiment were studied using Configurations 6 and 7, in which a linear variation of tip clearance from leading-to-trailing edge of 1/2-to-full and 3/4-to-full clearance height was used. In all three configurations the tip gap was modeled and contained eight cells. Although the number of grid cells in the tip clearance gap was decreased from 12 to 8 for these reduced clearance cases, the grids used in Configurations 5, 6, and 7 feature the same near-shroud spacing as that used in Configuration 3.

The clearance flow trajectory and penetration for the uniform 1/2 clearance case (Configuration 5) are presented in Figs. 9a and 10a. The trajectory in the blade-to-blade view is nearly identical to that of the 12-cell simulation for the full clearance height (Fig. 6b). The crosschannel view of the clearance flow in Fig. 10 indicates that the primary clearance flow fluid does not accumulate as much on the blade pressure surface in the 1/2 height simulation and is in closer agreement with the measured result shown in Fig. 3. However, the amount of secondary clearance flow has been greatly reduced in the 1/2 height case and is now underestimated relative to the measurements. A uniform reduction in tip clearance therefore generates minor changes in the primary clearance flow development and a stronger change in the secondary clearance flow strength.

The clearance flow trajectory and penetration from the 1/2-to-full clearance simulation (Configuration 6) are shown in Figs. 9b and 10b. The results shown in Fig. 10b indicate that the primary clearance flow displays only a weak tendency to accumulate on the pressure surface in the rear of the blade passage. The increased clearance height in the rear of the blade passage (relative to Configuration 5) allows a stronger secondary clearance flow to develop than in the 1/2-height, uniform clearance case. The results of the 3/4-to-full clearance height simulation lie between those for Configuration 6 and Configuration 3 and are not presented here. Configuration 6 therefore yields the simulation that most closely resembles the LDV data in the rear of the blade passage.

Results from Configurations 3, 5, and 6 are compared at the mid rotor/stator gap axial location in Fig. 11. The dashed line at 95% span marks the highest span at which LDV data were acquired (see Fig. 3). An assessment of the predicted and measured results at this downstream location shows that Configuration 6 yields the most satisfactory comparison with the measurements downstream of the blade as well. Comparison of the 1/2-to-full height and the uniform 1/2 height results (Figs. 11b and 11c) indicates that opening the clearance along the chord does not appreciably change the development of the primary leakage flow but strengthens the secondary leakage flow. This result is consistent with that of Adamczyk et al. (1993), who found that opening the clearance over the last 75% of a transonic rotor did not affect the clearance flow trajectory. Since increasing the clearance over the rear of the blade does not increase the strength of the primary clearance flow, these results may have an important ramification on operability in that tight tip clearances may only be necessary over the front portion of the blade. This might only be true for front-loaded blading. The impact of open clearance in the rear on stability must also be considered.

Because the primary and secondary clearance flow character of Configuration 6 as shown in Fig. 11b is in good qualitative agreement with the LDV data, the Configuration 6 results will be used for a more quantitative assessment of the accuracy of the predicted clearance flow.

Total temperature distributions in the tip region

CFD simulations of tip clearance flow generated during the ASME and AGARD assessment exercises on NASA Rotor 37 display a temperature excess in the blade tip region compared to temperatures measured downstream of the rotor with thermocouple probes, as summarized by Dunham and Meauze (1998), AGARD (1998), and Denton (1996). This overshoot has been attributed to an inability to correctly model the tip clearance flow and results in a significant underestimation of the efficiency in the outer 10-20% of blade span. However, the Rotor 37 temperature measurements were acquired far downstream (almost two chords) of the blade trailing edge. While thermocouple measurements of temperature can be acquired closer to the rotor trailing edge, conventional instrumentation often yields questionable results within one chord of the rotor due to the highly unsteady flowfield. Additionally any measurement made downstream of the rotor will be impacted by mixing, which is difficult to accurately predict with CFD. Assessments of CFD temperature predictions near the tip that are based on Rotor 37 may therefore not be accurate. The question therefore remains "Are the calculated temperature overshoots near the blade tip real?" To address this issue, the tangential velocity measured by the LDV system is used to calculate the total temperature within the tip clearance flow field using the Euler turbine equation. This derived fluid temperature is then used to provide a more

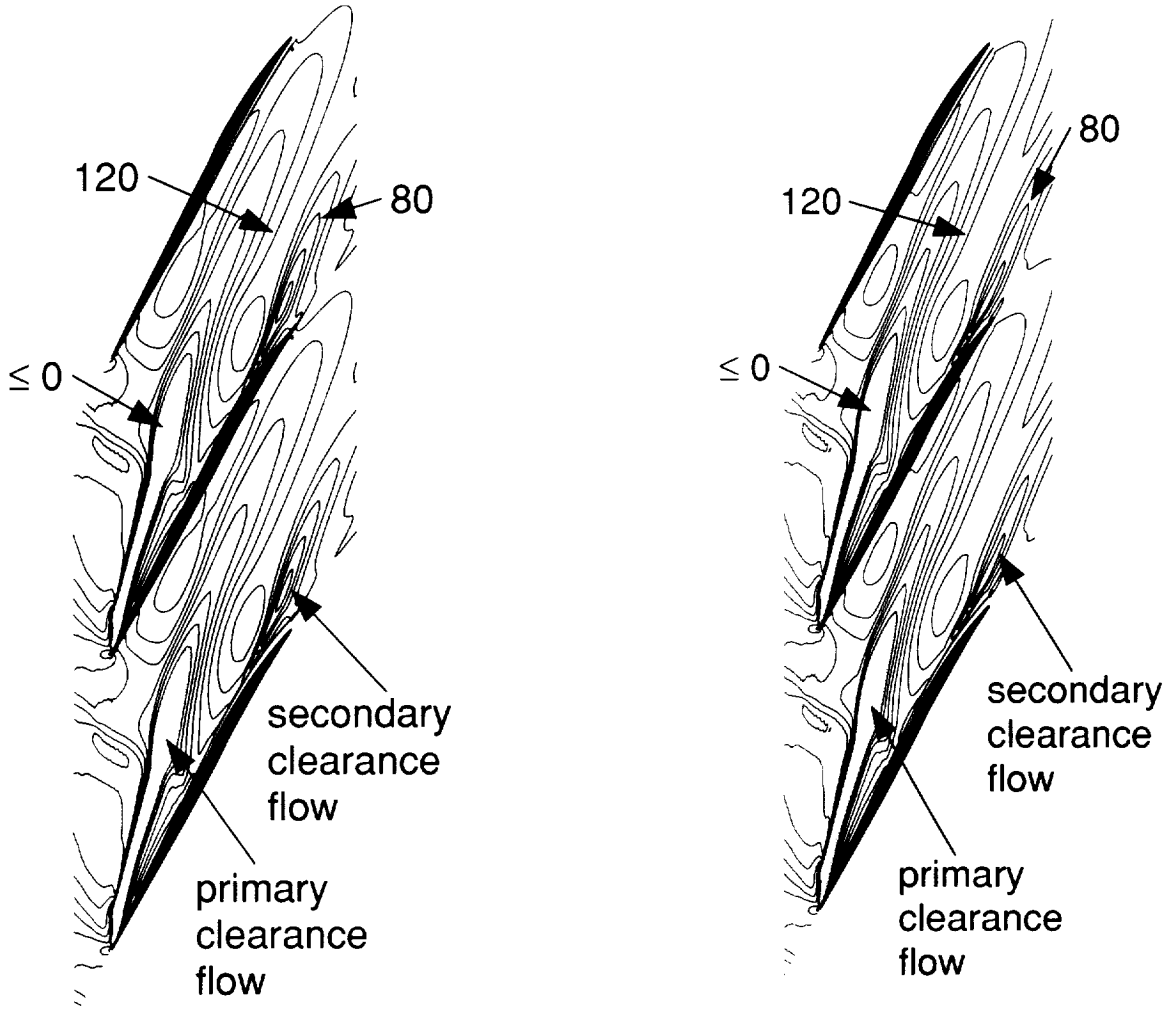

a) Configuration 5

b) Configuration 6

FIGURE 9. Axial velocity contours (starting at 0 m/s with 20 m/s interval) at the blade tip grid plane for configurations 5 and 6.

accurate assessment of the simulation fidelity than is possible using temperature measured far downstream.

One normally obtains the temperature predicted by a CFD simulation from the energy equation. However, in order to provide a back-to-back comparison with the derived fluid temperature as measured by the LDV system, we will obtain the CFD-predicted temperature using the predicted tangential velocity and the Euler turbine equation. This Euler-derived temperature will be slightly different near the shroud than that obtained from the energy equation. This is due to the fact that the Euler turbine equation assumes that rothalpy is conserved, an assumption that is not valid near the wall because of the shear work done on the fluid by the moving shroud wall in the relative frame of reference.

A quantitative comparison between the measured and predicted total temperature is obtained by displaying the results along a radial line that cuts through the center of the primary clearance flow at 92% blade chord. The Euler-derived measured temperature distribution is compared to the predicted (Configuration 6) temperature distribution in Fig. 12. Predicted temperature obtained from the energy equation and derived through the Euler equation are both shown The survey line for these results is shown in Fig. 11b. The local levels of the measured and predicted temperatures are somewhat different over the outer 20% of the blade span. All temperatures are therefore shifted such that the Euler-derived measured and predicted temperatures match at 80% span. The abscissa in Fig. 12 is therefore the normalized temperature excess:

$$(T(r) - T_{80})/T_{std} \qquad \text{(EQ 1)}$$

where T(r) is the temperature at radius r along the survey line, T_{80} is the temperature at 80% span along the survey line, and T_{std} = 288.2K. The largest difference between predicted normalized tem-

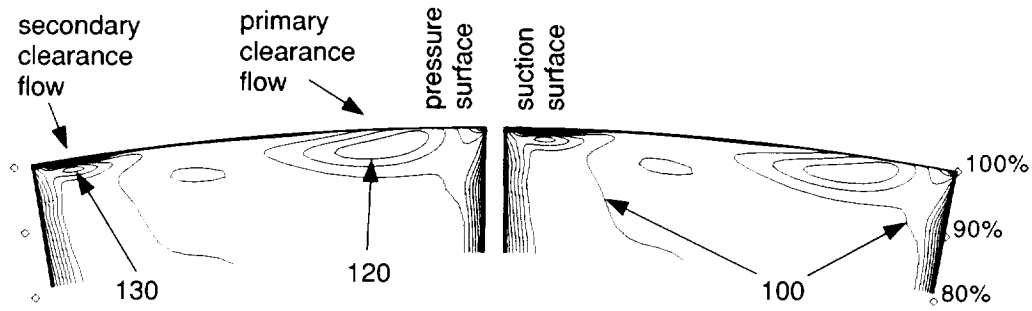

a) Configuration 5

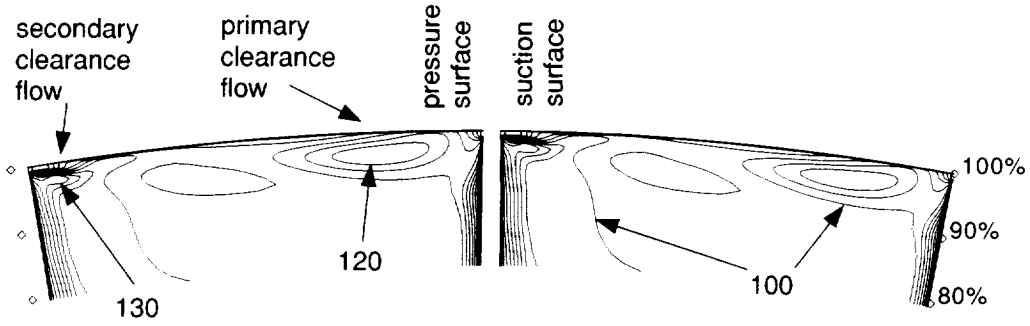

b) Configuration 6

FIGURE 10. Tangential velocity contours (10 m/s interval) for the outer 20% of span on the crosschannel surface at 92% rotor chord for configurations 5 and 6.

peratures obtained from the energy equation and the Euler turbine equation is 0.014 (4 K) and is confined to the last 1% of annulus height, which is approximately the clearance gap height.

The comparison shown in Fig. 12 confirms for the first time that a CFD simulation accurately predicts the local temperature excess associated with the increased turning in the clearance flow. The radial penetration of the clearance flow is also accurately predicted. The overall temperature rise of the rotor is 12% of the inlet total temperature for the operating condition considered here. The temperature excess within the clearance flow is therefore significant since its magnitude corresponds to 25-35% of the overall temperature rise. The results shown here suggest that temperature measurements derived from velocities measured within the rotor may provide the most reliable data for future assessments of CFD simulation accuracy.

Clearance flow trajectory effect on total temperature in the tip region

The results presented above indicate that the choice of near-wall grid spacing has a significant impact on the accurate prediction of the tip clearance flow development and the predicted non-uniform temperature distribution that exists in the rotor as a result of the clearance flow. In particular, detailed analysis of the simulations discussed above indicates that when the primary clearance flow accumulates on the adjacent blade pressure surface before reaching the rear of the blade passage, the low axial momentum fluid of the clearance flow is worked on by the adjacent rotor blade, further increasing its total temperature. This results in overprediction of the temperature rise in the tip region. Additionally, when the primary clearance flow accumulates on the adjacent blade pressure surface, the clearance flow merges with the pressure side of the blade wake and the total temperature excess in the clearance flow mixes very slowly downstream of the rotor. For axial blade spacings representative of those in modern multistage compressors, this results in a temperature excess entering the stator. Fig. 13a illustrates this effect at the stator leading edge location using results from Configurations 1 and 6. The absolute flow angle is also affected as shown in Fig. 13b. When the clearance flow accumulates on the pressure surface (Configuration1), the maximum pitch-averaged total temperature and the temperature at the casing are predicted to be higher than when the clearance flow does not impact on the pressure surface (Configuration 6). These errors result from an inaccurate prediction of the primary clearance flow trajectory and will contribute to an underprediction of rotor efficiency. In a multistage environment these errors can build in successive stages possibly resulting in a large overprediction of temperature at the blade tip and casing at the exit of the compressor.

DISCUSSION

The results presented above indicate that the only grid con-

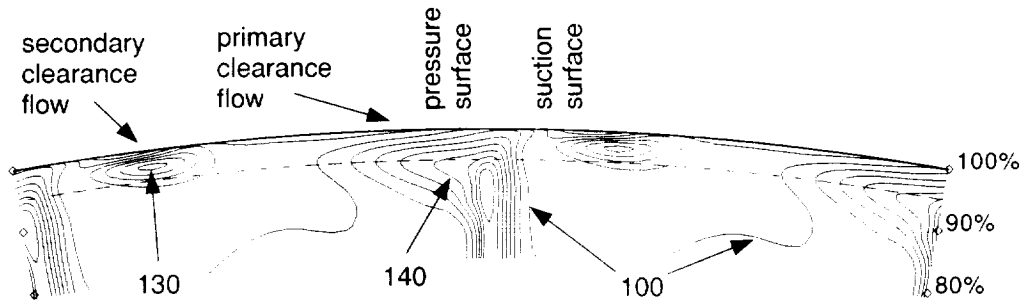

a) Configuration 3

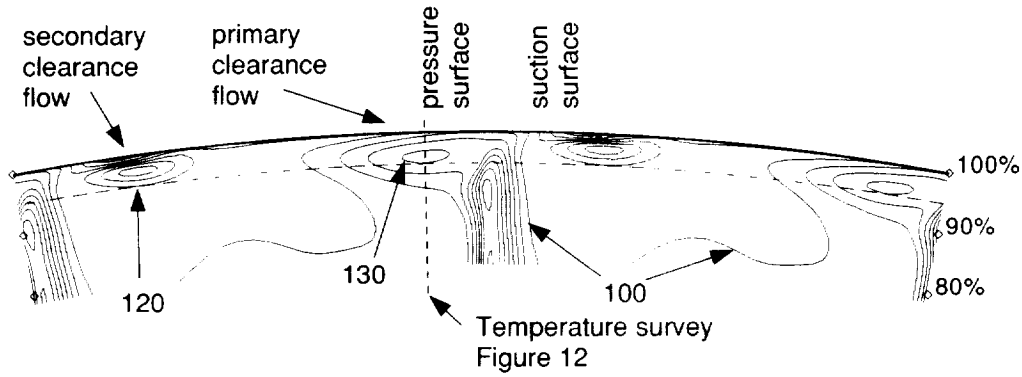

b) Configuration 6

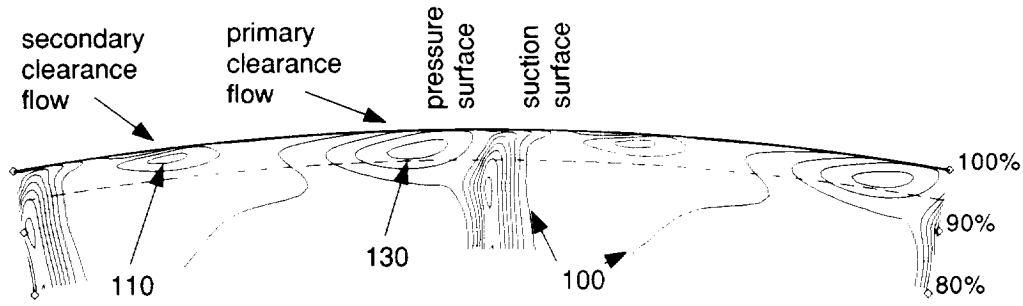

c) Configuration 5

FIGURE 11. Tangential velocity contours (10 m/s intervals) for the outer 20% of span on the crosschannel surface at mid rotor/stator gap location.

figuration change that significantly alters the trajectory of the clearance flow is the increase in near-shroud grid resolution between Configurations 1 and 3. The increased resolution of Configuration 3 places four grid cells across the same distance from the wall as covered by the first grid cell in Configuration 1 while leaving the grid cell size at the blade tip virtually unchanged. A case with higher near-shroud grid resolution than Configuration 3 was also run but showed no further change in the clearance flow trajectory, indicating that the grid resolution of Configuration 3 is sufficient to achieve a grid-independent solution. The incoming boundary layer on the shroud and the computed wall shear stress are nearly identical in the Configuration 1 and 3 solutions, indicating that changes in the clearance flow trajectory are not due to different inlet conditions. The solutions were examined closely for any indication of numerical problems in the tip clearance region. No evidence of odd-even decoupling or inconsistencies in the wall shear stress calculated by the turbulence model was found. To understand why the increased spatial resolution of Configuration 3 has such a marked impact on the clearance flow trajectory, we therefore need to consider the fluid mechanic processes at work in the early development of the clearance flow.

Dean (1954), Storer and Cumpsty (1991), Chen et al. (1991)

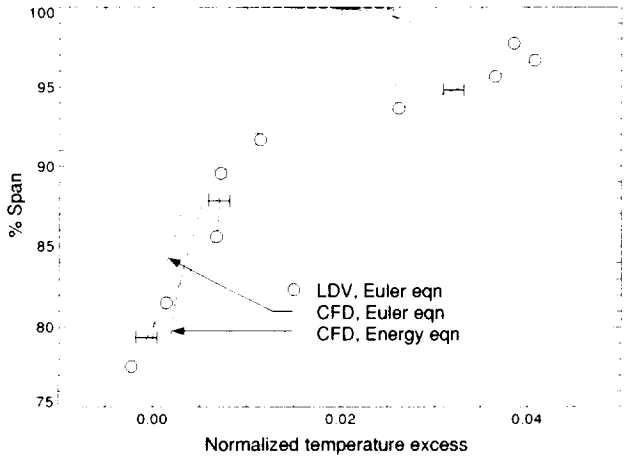

FIGURE 12. Total temperature excess of the clearance flow at 92% rotor chord along the survey line shown in Figure 11b.

and others have proposed that the formation of the clearance flow jet is predominantly an inviscid phenomenon driven by the pressure difference across the blade tip, wherein the over-tip leakage jet and its associated free shear layer roll up into the main clearance vortex. While this is a good approximation in most cases, it neglects the fact that the tip leakage flow consists of two shear layers: i) the free shear layer formed between the over-tip leakage jet and the main through flow; ii) a wall-bounded shear layer formed between the leakage jet and the shroud. The wall-bounded shear layer will be present whenever there is a velocity difference between the over-tip leakage jet and the shroud in the relative frame of reference. Chima (1998) alluded to the presence of the wall-bounded shear layer based on the trajectory of flow tracers he released at mid-height in the clearance gap, but did not investigate the interaction between this shear layer and the free shear layer at the blade tip.

The role played by the wall-bounded shear layer in determining the trajectory of the main clearance vortex is illustrated in Figure 14. The axial velocity distribution in a blade-to-blade plane that is 2 grid cells from the shroud is shown in the upper half of Fig. 14. This plane is located just 6% of the clearance gap height from the shroud (99.95% of the annulus height). Blue regions denote areas in which fluid is moving upstream (negative axial velocity). This fluid is the over-tip leakage flow and its upstream motion has been well-documented by previous investigators. The red region denotes an area in which fluid is moving downstream with an axial velocity which is appreciably higher than that in the incoming boundary layer at this immersion. The origin of this high positive axial velocity can be understood by viewing the flow field on a z-r cutting plane denoted by the white line. The projection of the relative velocity vectors onto this plane is shown in the lower half of Fig. 14 as viewed in the negative θ direction. The blade suction surface appears on the left edge of the plot. The velocity vectors are colored by their θ-component of vorticity. The over-tip leakage jet forms a vortex centered at the point P. The sign of the θ-component of vorticity is negative (rotation in the clockwise direction in Fig. 14b). The wall bounded shear layer appears as the color purple in Fig. 14b. In the present case the sign of the vorticity in this shear layer is positive (counterclockwise rotation in Fig. 14b). This shear layer initially occupies only about 20% of the clearance height, but is then pulled away from the shroud by the vortex centered at P and forms a vortex centered at point I which we will call the "induced vortex". The paths of the primary clearance vortex (centered at P) and the induced vortex (centered at I) are shown in the blade-to-blade view in the upper half of Fig. 14.

The Configuration 1 solution (not shown here) indicates that the wall-bounded shear layer is not adequately resolved by the near-shroud grid spacing used in Configuration 1, while the results shown in Fig. 14 indicate that it is adequately resolved by that used in Configuration 3. To understand why a change in grid spacing alters the trajectory of the main clearance flow, we must consider its impact on the strength (as measured by their circulation) of the primary and induced vortices. Both the primary and induced vortices have an image vortex in the shroud to satisfy the condition of zero normal velocity at the shroud. The mutual interaction between the primary vortex and its image acts to move the primary vortex axially upstream and away from the blade suction surface (to the right in the lower half of Fig. 14). Conversely, the mutual interaction between the induced vortex and its image acts to move the induced vortex axially downstream toward the blade suction surface. The circulation in each vortex will determine the equilibrium position of the primary and induced vortices. The circulation for each vortex (in arbitrary units) is:

Configuration	1	3
Primary vortex circulation, P	199, 200	223,800
Induced vortex circulation, I	14, 200	77, 300
Ratio, I/P	7%	35%

The circulation of the primary vortex increases by about 10% in Configuration 3 relative to Configuration 1. Taken by itself, this change would act to move the primary vortex further upstream, away from the suction surface. However, this change is more than offset by the increased strength of the induced vortex in Configuration 3. The net effect of the changes in vortex strength between Configurations 1 and 3 is therefore a movement of the primary/induced vortex pair downstream toward the suction surface, which alters the trajectory of the primary clearance flow.

It is instructive to consider under what conditions the wall-bounded shear layer plays a determining role in the development of the tip clearance flow. The relationship between the leakage jet velocity and the shroud velocity in the relative frame is shown in Fig. 15. The velocity vector lengths are drawn to scale, using the blade tip speed and the leakage velocity at mid-height in the clearance gap from the Configuration 3 simulation. Let us define a normalized velocity difference between the shroud and leakage jet by the parameter:

$$VD = (Vjet - Vwall\cos\gamma)/(Vwall) \qquad \text{(EQ 2)}$$

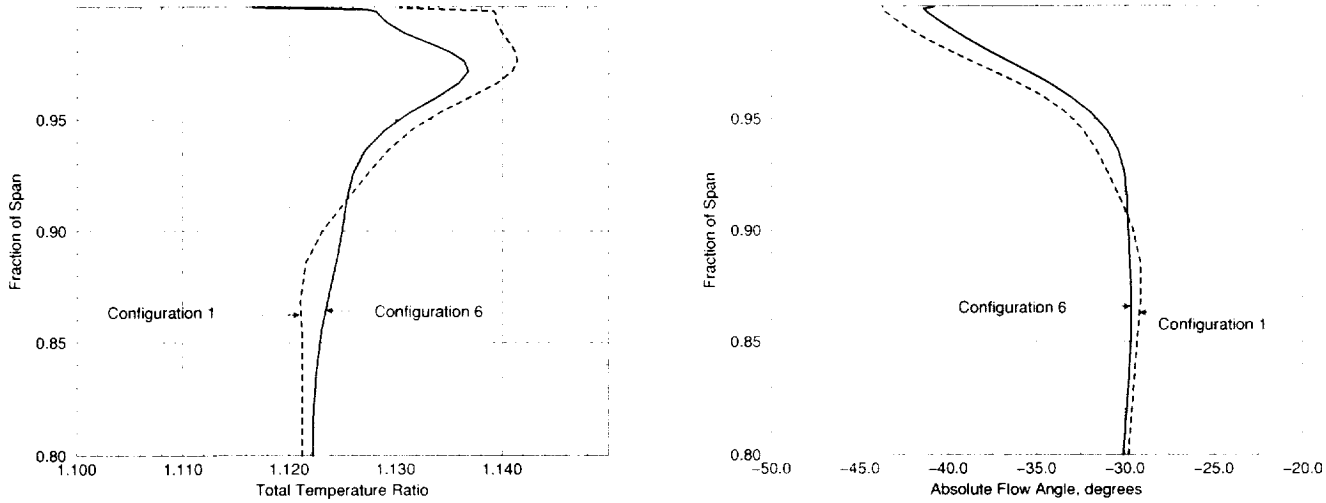

FIGURE 13. Pitch averaged total temperature and tangential flow angle profiles at the stator leading edge plane.

where *Vwall* is the blade tip speed and γ is the difference between the relative flow angle of the leakage jet and the tangential direction. Evaluating this parameter for Rotor 35 at the 80% speed, peak efficiency operating condition simulated herein we find VD= 0.40. The sign of this velocity difference determines the sign of the vorticity in the wall-bounded shear layer. When the velocity difference is greater than zero, as in the present case, the θ-component of vorticity is positive and is of opposite sense to that in the free shear layer and the incoming shroud boundary layer. When the velocity difference is less than zero, the θ-component of vorticity in the wall shear layer will be of the same sense as that in the free shear layer. When this velocity difference is small, the wall-bounded shear layer will be weak and will not exert a strong influence on the primary leakage flow. In such cases an inviscid approximation can be used for the leakage jet and a computational grid with relatively few points in the clearance gap will yield an accurate leakage flow simulation.

To check the generality of the criteria set forth above, two additional compressor rotors were simulated. In each case solutions were generated with near-shroud grid spacings representative of those used in Configurations 1 and 3 of the present work, and the results were analyzed for both the presence of the induced vortex and for changes in the primary clearance flow trajectory as grid resolution was increased. The first additional case was Rotor 35 at the design speed, near peak efficiency operating condition. The total pressure ratio, efficiency, and tip speed for this case are 1.90, 86%, and 454 m/sec respectively. The velocity difference parameter for this case is VD=0.2 and the solutions show the presence of an induced vortex which alters the clearance flow trajectory when adequate near-shroud grid resolution is used. The second additional case was the rotor in the NASA-Lewis Low Speed Axial Compressor (LSAC), which is a low-speed four-stage model of the General Electric Energy Efficient Engine compressor rear stages (Barankiewicz and Hathaway, 1998). The total pressure ratio and tip speed for this case are 1.042 and 61 m/sec respectively. The velocity difference parameter for the LSAC is VD=0.05 and refining the grid in the tip gap had no significant impact on the clearance flow. In summary, values of the velocity difference parameter on the order of 0.2 or higher appear to indicate the presence of a wall-bounded shear layer of sufficient strength to impact the primary clearance flow trajectory.

In the above discussion the velocity difference parameter, VD, was evaluated using information obtained from the CFD solution itself. When starting the analysis of a new rotor, it would be useful to have an *a priori* estimate of VD to serve as guidance in selecting the proper near-shroud grid resolution. Such an estimate can be obtained using the leakage jet velocity approximation provided by Khalsa (1996). Based on the formula of Khalsa but in the relative reference frame the leakage flow angle relative to the blade stagger angle for incompressible flow is:

$$\alpha = \operatorname{atan}\left(\frac{Vl}{Vsw}\right) = \operatorname{atan}\left(\sqrt{\frac{(P_{Trel} - P_{ss})}{(P_{Trel} - P_{ps})}}\right) \qquad \text{(EQ 3)}$$

where

Vl= leakage velocity normal to blade surface

Vsw= leakage velocity tangent to blade surface

Ptrel= relative total pressure on pressure surface

Pss= static pressure on suction surface

Pps= static pressure on pressure surface

Noting that *Vjet* and *Vwall* in Eqn. 2 are equal to *Vl*/sinα and *Utip* (the blade speed) respectively, one can obtain the following expression for VD involving only blade geometry and surface loading parameters,

$$VD = (Vl - Utip\sin(\beta + \alpha)\sin\alpha)/(Utip\sin\alpha) \qquad \text{(EQ 4)}$$

where β is the stagger angle. For incompressible flow the leakage velocity can be computed as (ρ is density):

$$Vl = \sqrt{(2(P_{Trel} - P_{ss}))/\rho_{ss}} \qquad \text{(EQ 5)}$$

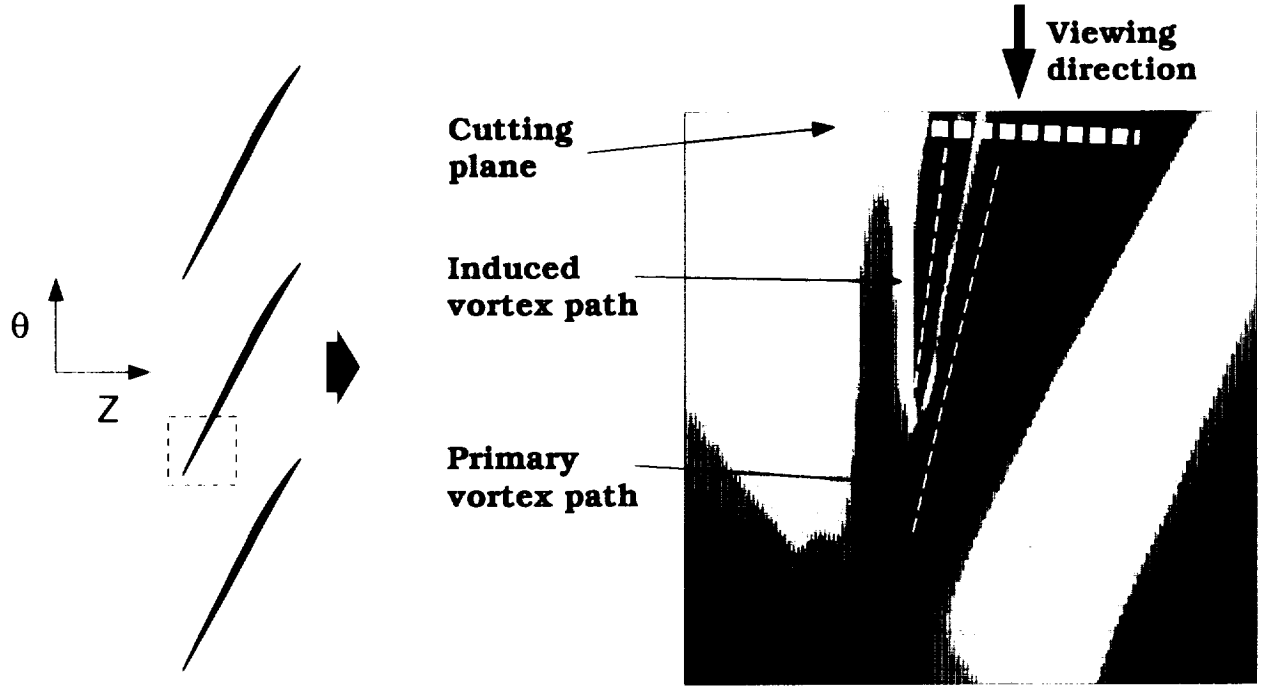

a) Axial velocity at 6% of clearance gap height from the shroud.

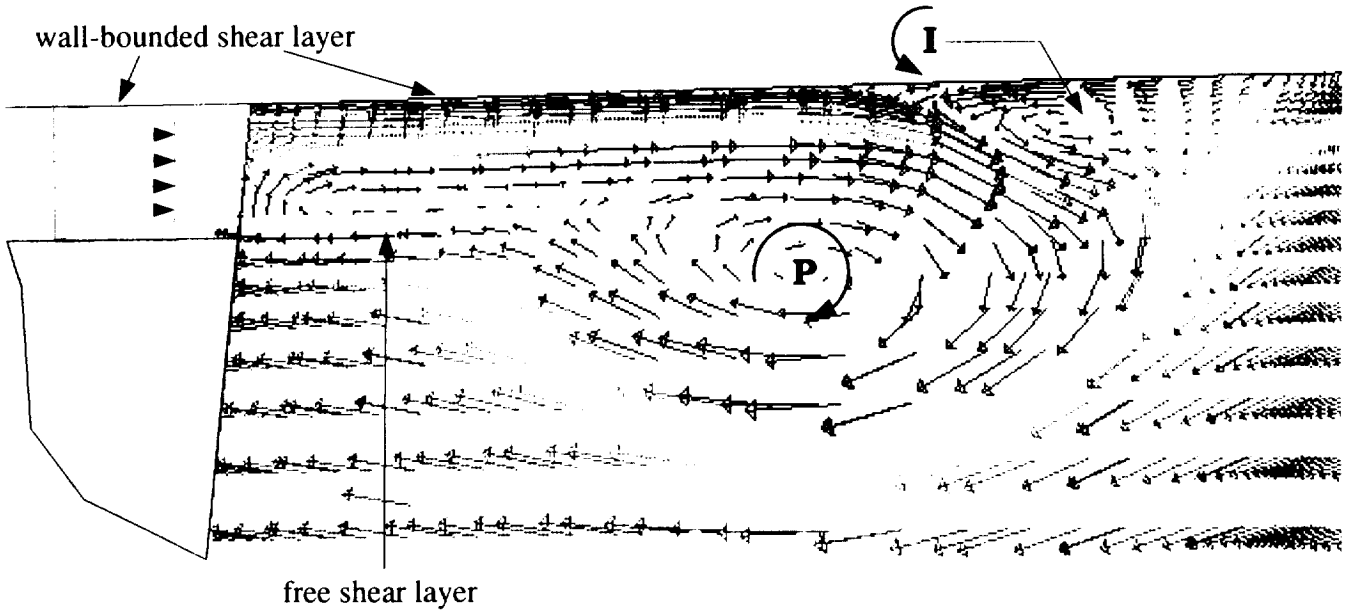

b) Velocity vectors on z-r cutting plane, colored by the θ-component of vorticity.

FIGURE 14. Visualization of primary and induced clearance vortices.

Equations 3, 4, and 5 can be evaluated with information obtained from the blade design process so that the value of the velocity difference parameter is known prior to grid generation for a Navier-Stokes simulation.

CONCLUSIONS

The tip clearance flow field of NASA Rotor 35 was simulated using a Navier-Stokes turbomachinery solver to determine the effect of grid topology and tip gap treatment on solution fidelity. Detailed laser anemometer measurements of the rotor tip clearance flow field were used as a basis for comparison of clearance flow trajectory and radial extent as simulated and as actually observed in tests. The following conclusions are drawn from these comparisons:

- Gridding the tip gap does not yield any significant advantages in solution accuracy compared to using a simple tip clearance model. Accurate clearance flow predictions can be generated without gridding the gap and we recommend that the computationally efficient tip clearance model of Kirtley et al. (1990) be used for thin blades typical of most compressors.
- Adequate resolution of a wall-bounded shear layer formed between the leakage jet and the shroud is key to achieving accurate clearance flow predictions. This shear layer forms due to the net relative velocity difference between the leakage jet and the shroud. The primary clearance flow rolls this shear layer into an induced vortex which impacts the trajectory of the primary clearance flow. For cases where the net relative velocity difference between the leakage jet and shroud is large we recommend careful attention to grid resolution near the casing.
- Previous assessments of CFD simulation accuracy using thermocouple temperature measurements acquired far downstream of the rotor have incorrectly concluded that CFD simulations overpredict the temperature increase at the rotor tip. By comparing CFD-predicted temperature within the rotor to that derived from the LDV-measured tangential velocity using the Euler turbine equation, we have shown that CFD simulations can accurately predict the total temperature increase at the tip of the rotor if the grid topology in the clearance region is handled properly.
- The magnitude of the total temperature excess within the clearance flow predicted by the CFD is strongly influenced by the trajectory of the clearance flow. Excessive temperature rise in the tip caused by incorrect clearance flow trajectory leads to large overpredictions of tip and casing temperature in the single stage compressor studied herein. These errors can be expected to multiply in multistage simulations.

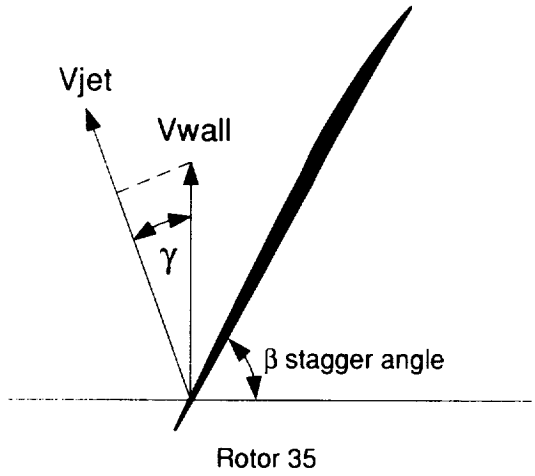

FIGURE 15 Relation of the clearance jet velocity and the shroud-wall velocity in the relative reference frame. The projection of the wall velocity into a direction which is parallel to the jet is shown by a dashed line.

- Larger clearances in the rear portion of the blade are not detrimental for highly-loaded airfoils over the range of clearances investigated here (clearance/chord < 1/3%). The clearance gap height over the front part of the rotor chord has a weak influence on the primary clearance flow trajectory. The clearance height at the trailing edge influences the strength of the secondary clearance flow that emerges in the last 25% of chord, but has little influence on the primary clearance flow.

REFERENCES

Adamczyk, J.J., Celestina, M.L., Beach, T.A., and Barnett, M., 1990, "Simulation of Three-Dimensional Viscous Flow Within a Multistage Turbine," ASME Journal of Turbomachinery, Vol. 112, pp. 370-376.

Adamczyk, J.J., Celestina, M.L., and Greitzer, E.M., 1993, "The Role of Tip Clearance in High-Speed Fan Stall," ASME Journal of Turbomachinery, Vol. 115, pp. 28-38.

AGARD, 1998, "CFD Validation for Propulsion System Components," edited by J. Dunham, AGARD-AR-355.

Barankiewicz, W.S., and Hathaway, M.D., 1998, "Impact of Variable-Geometry Stator Hub Leakage in a Low Speed Axial Compressor," ASME 98-GT-194.

Chen, G.T., Greitzer, E.M., Tan, C.S., and Marble, F.E., 1991, "Similarity Analysis of Compressor Tip Clearance Flow Structure," ASME Journal of Turbomachinery, Vol. 113, pp. 260-271.

Chima, R. V., 1998, "Calculation of Tip Clearance Effects in a Transonic Compressor Rotor," ASME Journal of Turbomachinery, Vol. 120, pp 131-140.

Dawes, W.N., 1987, "A Numerical Analysis of the Three-Dimensional Viscous Flow in a Transonic Compressor Rotor and Comparison with Experiment," ASME Journal of Turbomachinery, Vol. 109, pp. 83-90.

Dean, R.C., Jr., 1954, The Influence of Tip Clearance on Boundary-Layer Flow in a Rectilinear Cascade," MIT Gas Turbine Laboratory Report No. 27-3.

Denton, J.D., 1996, "Lessons Learned from Rotor 37," presented at the 3rd International Symposium on Experimental and Computational Aerothermodynamics of Internal Flows (ISAIF), Beijing, China, September 1-6, 1996.

Dunham, J., and Meauze, G., 1998, "An AGARD Working Group Study of 3D Navier-Stokes Codes Applied to Single Turbomachinery Blade Rows," ASME Paper No. 98-GT-50.

Gerolymos, G.A. and Vallet, I., 1998, "Tip-Clearance and Secondary Flows in a Transonic Compressor Rotor," ASME Paper 98-GT-366.

Hoying, D.A., Tan, C.S., Vo, H.D., and Greitzer, E.M., 1998, "Role of Blade Passage Flow Structures in Axial Compressor Rotating Stall Inception," ASME Paper No. 98-GT-588.

Khalsa, A.S., "Endwall Blockage in Axial Compressors," PhD Dissertation, Massachusetts Institute of Technology, June 1996.

Kirtley, K.R., Beach, T.A., and Adamczyk, J.J., 1990, "Numerical Analysis of Secondary Flow in a Two-Stage Turbine," Paper No. AIAA-90-2356.

Reid, L. and Moore, R. D., 1978, "Performance of Single-Stage Axial-Flow Transonic Compressor With Rotor and Stator Aspect Ratios of 1.19 and 1.26, Respectively, and with Design Pressure Ratio of 1.82," NASA TP 1338.

Shabbir, A., Zhu, J., and Celestina, M.L., 1996, "Assessment of Three Turbulence Models in a Compressor Rotor," ASME Paper No. 96-GT-198.

Shabbir, A., Celestina, M.L., Adamczyk, J.J., and Strazisar, A.J., 1997, "The Effect of Hub Leakage Flow on Two High Speed Axial Compressor Rotors," ASME Paper No. 97-GT-346.

Storer, J.A., and Cumpsty, N.A., 1991, "Tip Leakage Flow in Axial Compressors," ASME Journal of Turbomachinery, Vol. 113, pp. 252-259.

Strazisar, A. J., Wood, J. R., Hathaway, M. D., and Suder, K. L., 1989, "Laser Anemometer Measurements in a Transonic Axial-Flow Fan Rotor," NASA TP 2879.

Suder, K. L. and Celestina, M. L., 1996, "Experimental and Computational Investigation of the Tip Clearance Flow in a Transonic Axial Compressor Rotor," ASME Journal of Turbomachinery, Vol. 118, pp. 218-229.

Van Zante, D.E., Adamczyk, J.A., Strazisar, A.J., and Okiishi, T.H., 1997, "Wake Recovery Benefit in a High-Speed Axial Compressor," ASME Paper 97-GT-535.

Wisler, D.C., 1985, "Loss Reduction in Axial Flow Compressors through Low-Speed Model Testing," ASME Journal of Turbomachinery, Vol. 107, pp. 354-363.

APPENDIX

Operating range predictions

Hoying et. al (1998) and Adamczyk et. al (1993) suggest that rotor stall occurs when the tip clearance vortex spills forward of the leading edge, thereby linking the clearance vortex path to rotor stability. Since our tip grid topology impacts the clearance trajectory this also implies a link between our grid topology and the predicted stability. Figure 16 shows the 80% speed line for Rotor 35 calculated with configuration 1 and 3 grids. The stall point for both simulations and the experiment are marked with arrows. The results confirm a large effect on predicted operating range with configuration 3 showing a much better match to experiment.

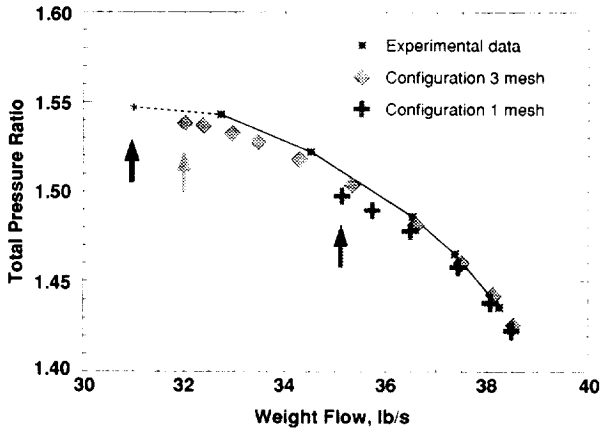

FIGURE 16. Comparison of computed and measured operating range for Rotor 35 at 80% speed.

Figure 17 shows the design speed operating line for Rotor 35 calculated with configuration 1 and 3 grids. Configuration 3 again shows better operating range prediction when compared to the experiment.

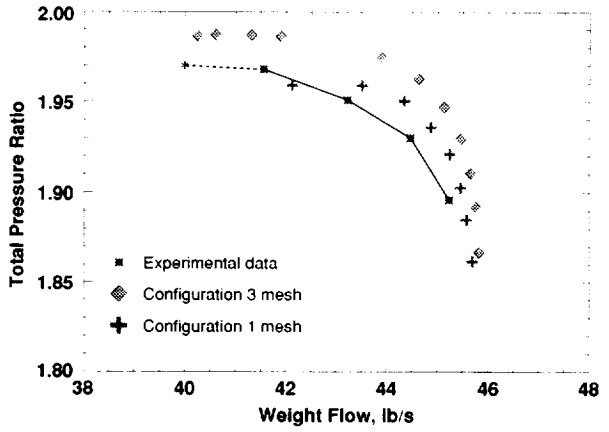

FIGURE 17. Comparison of computed and measured operating range for Rotor 35 at design speed.

The simulation results in Figure 16 and 17 indicate that the induced vortex has a strong impact on the rotor stability, suggesting that rotor stability can be enhanced by increasing the strength of the induced vortex.

LDV data

LDV data from the crosschannel surveys is presented as shaded contours plots of absolute tangential and axial velocity for the peak efficiency operating condition. Figures 18 and 19 present the data for 80% speed. Figure 20 shows data for design speed. This data is available in tabular form by contacting the authors.

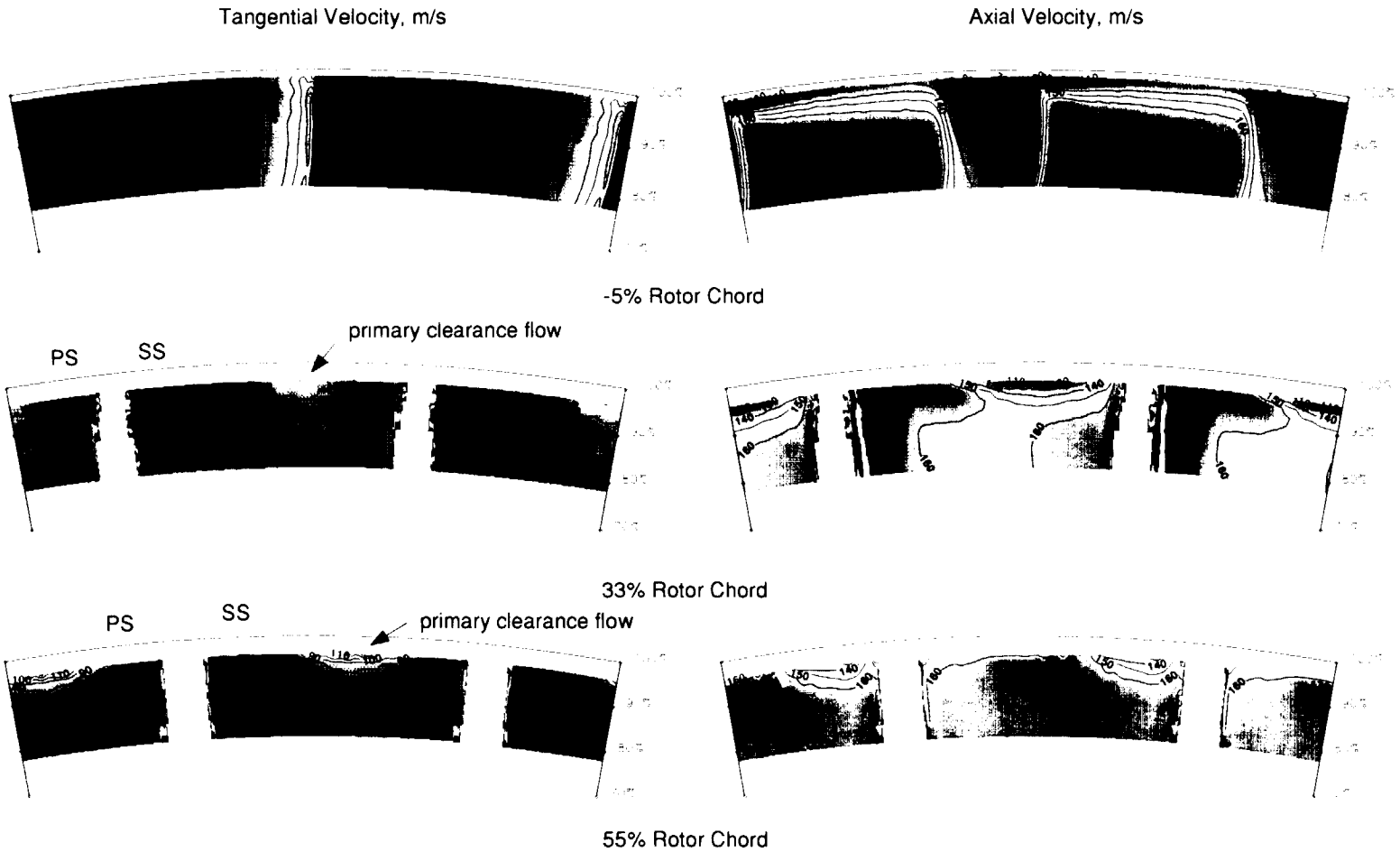

FIGURE 18. Rotor 35 LDV data for 80% speed. Part A.

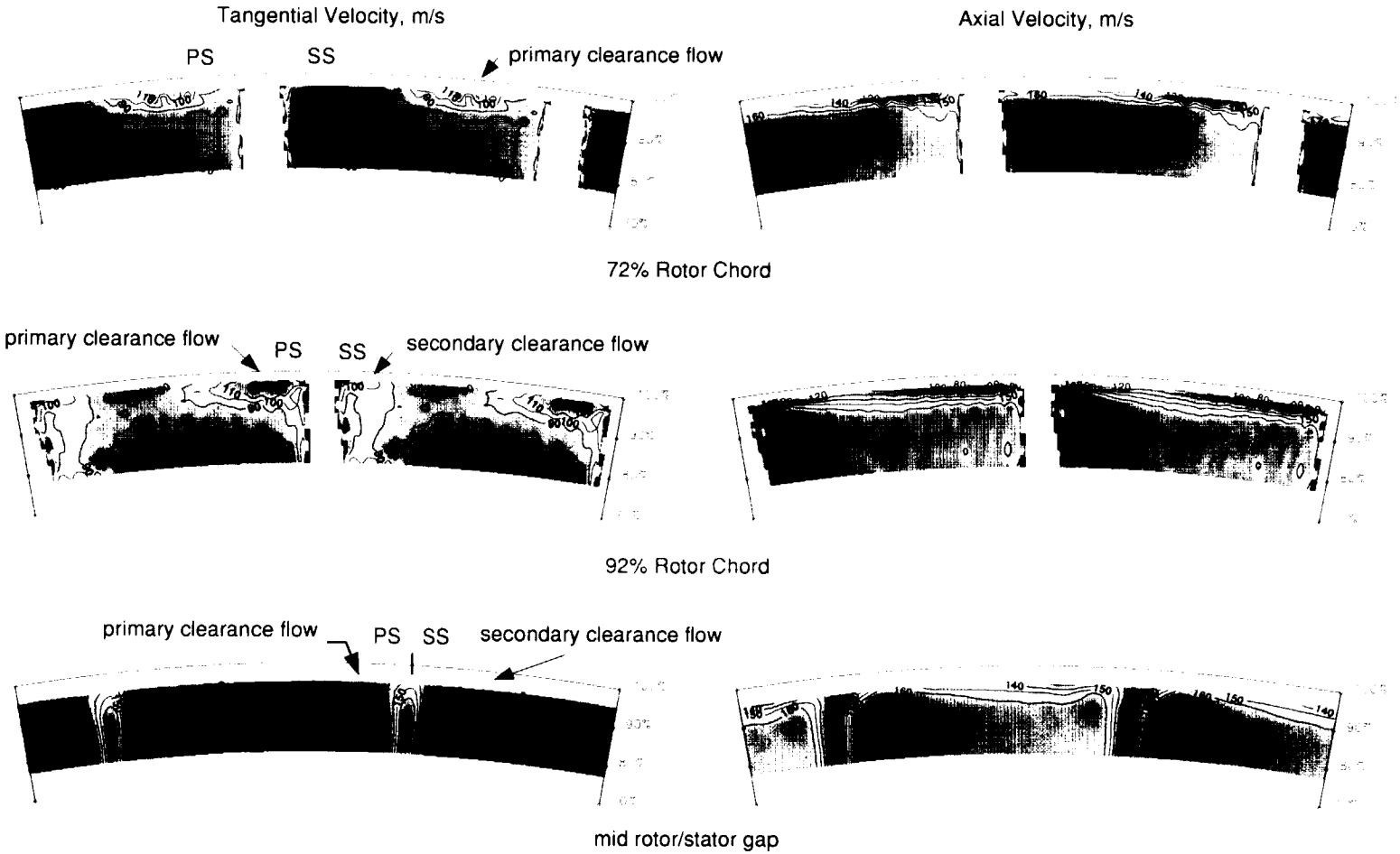

FIGURE 19. Rotor 35 LDV data for 80% speed. Part B.

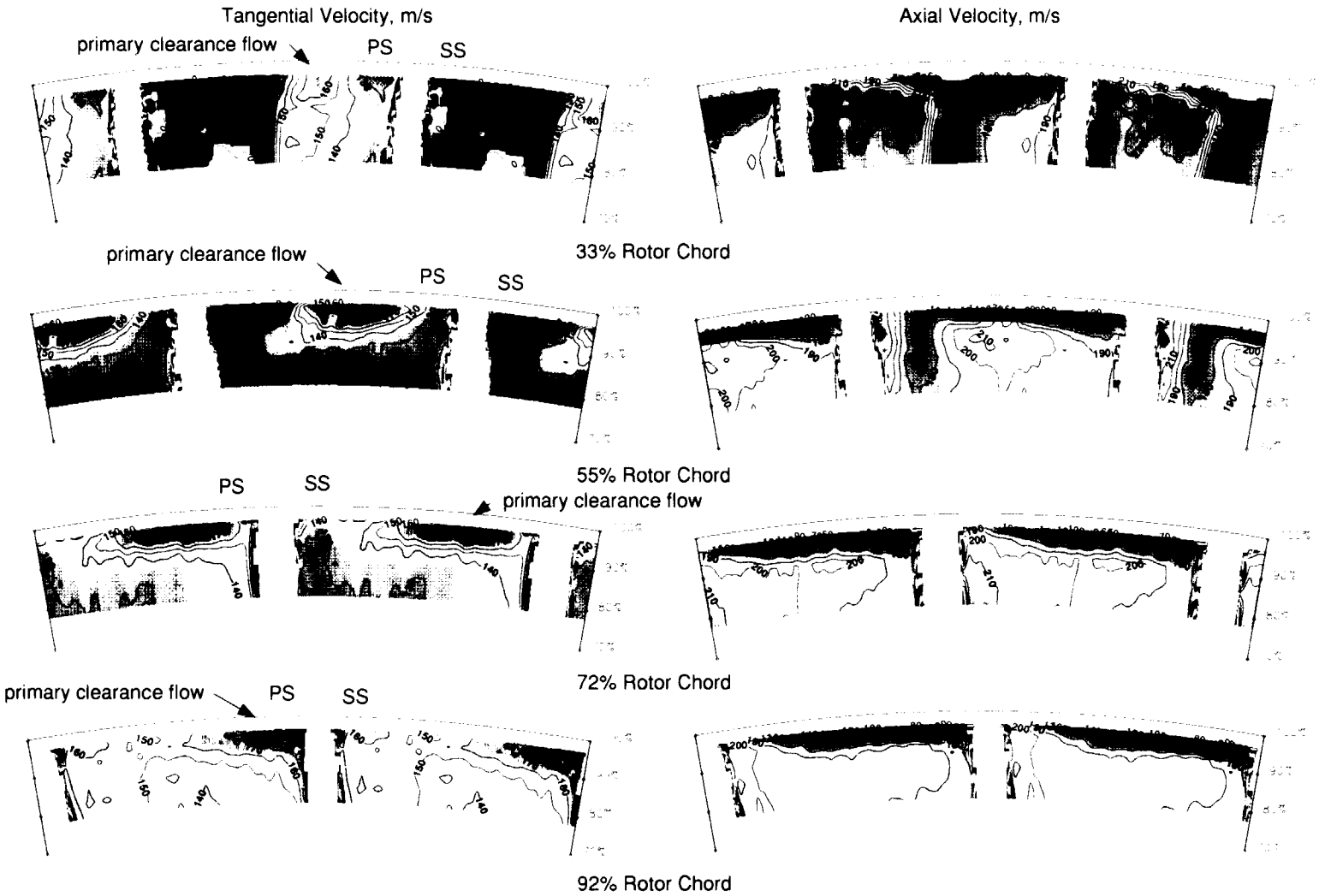

FIGURE 20. Rotor 35 LDV data for design speed.

REPORT DOCUMENTATION PAGE

Form Approved
OMB No. 0704-0188

1. AGENCY USE ONLY (*Leave blank*)	2. REPORT DATE	3. REPORT TYPE AND DATES COVERED
	September 2000	Technical Memorandum

4. TITLE AND SUBTITLE

Recommendations for Achieving Accurate Numerical Simulation of Tip Clearance Flows in Transonic Compressor Rotors

5. FUNDING NUMBERS

WU-523-26-33-00

6. AUTHOR(S)

Dale E. Van Zante, Anthony J. Strazisar, Jerry R. Wood, Michael D. Hathaway, and Theodore H. Okiishi

7. PERFORMING ORGANIZATION NAME(S) AND ADDRESS(ES)

National Aeronautics and Space Administration
John H. Glenn Research Center at Lewis Field
Cleveland, Ohio 44135-3191

8. PERFORMING ORGANIZATION REPORT NUMBER

E-12395

9. SPONSORING/MONITORING AGENCY NAME(S) AND ADDRESS(ES)

National Aeronautics and Space Administration
Washington, DC 20546-0001

10. SPONSORING/MONITORING AGENCY REPORT NUMBER

NASA TM—2000-210347

11. SUPPLEMENTARY NOTES

Prepared for the International Gas Turbine Institute Exposition sponsored by the American Society of Mechanical Engineers, Indianapolis, Indiana, July 7–10, 1999. Dale E. Van Zante, Anthony J. Strazisar, and Jerry R. Wood, NASA Glenn Research Center; Michael D. Hathaway, U.S. Army Research Laboratory, NASA Glenn Research Center; Theodore H. Okiishi, Iowa State University, Ames, Iowa 50011-2010. Responsible person, Dale E. Van Zante, organization code 5810, (216) 433-3640.

12a. DISTRIBUTION/AVAILABILITY STATEMENT

Unclassified - Unlimited
Subject Category: 07 Distribution: Nonstandard

This publication is available from the NASA Center for AeroSpace Information, (301) 621-0390.

12b. DISTRIBUTION CODE

13. ABSTRACT ***(Maximum 200 words)***

The tip clearance flows of transonic compressor rotors are important because they have a significant impact on rotor and stage performance. While numerical simulations of these flows are quite sophisticated, they are seldom verified through rigorous comparisons of numerical and measured data because these kinds of measurements are rare in the detail necessary to be useful in high-speed machines. In this paper we compare measured tip-clearance flow details (e.g. trajectory and radial extent) with corresponding data obtained from a numerical simulation. Recommendations for achieving accurate numerical simulation of tip clearance flows are presented based on this comparison. Laser Doppler Velocimeter (LDV) measurements acquired in a transonic compressor rotor, NASA Rotor 35, are used. The tip clearance flow field of this transonic rotor was simulated using a Navier-Stokes turbomachinery solver that incorporates an advanced k-ε turbulence model derived for flows that are not in local equilibrium. Comparison between measured and simulated results indicates that simulation accuracy is primarily dependent upon the ability of the numerical code to resolve important details of a wall-bounded shear layer formed by the relative motion between the over-tip leakage flow and the shroud wall. A simple method is presented for determining the strength of this shear layer.

14. SUBJECT TERMS	15. NUMBER OF PAGES
Axial compressor; Tip clearance flow; Laser doppler velocimetry	27
	16. PRICE CODE: A03

17. SECURITY CLASSIFICATION OF REPORT	18. SECURITY CLASSIFICATION OF THIS PAGE	19. SECURITY CLASSIFICATION OF ABSTRACT	20. LIMITATION OF ABSTRACT
Unclassified	Unclassified	Unclassified	